Application Notes

ExoMars Rover PanCam: Autonomy and Computational Intelligence

Peter Yuen,
Mullard Space Science Laboratory, UCL, UK

Yang Gao, *Surrey Space Centre, University of Surrey, UK*

Andrew Griffiths, Andrew Coates, Jan-Peter Muller, Alan Smith, Dave Walton, Craig Leff, and Barry Hancock
Mullard Space Science Laboratory, UCL, UK

Dongjoe Shin, *Computer Laboratory, University of Cambridge, UK*

I. Introduction

As a part of the Aurora programme for Mars exploration, funded by the United Kingdom Space Agency (UKSA) and European Space Agency (ESA), the UK contributes to the Exobiology on Mars (ExoMars) rover science and engineering programme, with a scheduled launch in 2018; Hence, our Panoramic Camera (PanCam) [9][15] research and development (R&D) is timely. PanCam consists of two stereo Wide Angle Cameras (WAC) and one High Resolution Camera (HRC). While the development is still ongoing, we used funding awarded by the University College London (UCL) Graduate School to conduct investigations in the Himalayas and at Mount Everest Base Camp (EBC), according to the ExoMars rover Reference Surface Mission (RSM). The investigations included capturing stereo and high resolution images using stereo WAC emulators and HRC emulator at altitudes 3490 m, 5150 m and above. Images from different WAC filters, and color images from HRC were acquired at various Pan and Tilt Unit (PTU) mast positions. Our investigation results show significant reduction in data volume with minimum loss in image quality. Furthermore, we introduce a novel autonomous and computational intelligent system called Mission-Specific Data Processor (MSDP) for the rover. It includes PanCam, Visual Data Fusion (VDF), Learning-enabled Object Detection (LOD), Self-Learning Agent (SLA) [22], and Environment Model Library (EML) as part of the rover's computational intelligence [7].

UCL Mullard Space Science Laboratory (MSSL) has been involved in the ExoMars mission since 2003. It includes scientific research, detailed design and development of PanCam as shown in Figure 1. Given the Martian atmospheric pressure of less than 14 hectopascal (hPa), high UV flux 50 W/m^2 [21], extreme temperature fluctuations between −120 °C and +27 °C in a Sol (one Sol is equivalent to 24 hr 39 min 35.24409 sec), and at 300 parts per million (i.e. 300 mg/kg) Water Vapor Fraction (WVF) is more of a trace constituent; we selected the Himalayan region and EBC to conduct our investigations in Summer 2010, a year after the National Aeronautics and Space Administration (NASA) ran their experiments at Mount Everest [6]. The chosen sites for investigation have typical pressure 483 hPa, UV flux 30 W/m^2, daily temperature varies between −50 °C at night and +46 °C during daytime, and WVF 1100 mg/kg (dry air).

ExoMars rover RSM is a set of daily plans [2] [13] which are performed within the nominal surface mission duration as defined in Table 1. It consists of PanCam operational timeline sequences in a number of the Sols; these sequences handle functions such as WAC and HRC autoexposure, autofocus for HRC, images acquisition, iteration, time delay, thermal control and cameras mode switching.

As shown in Figure 2(a) and (b), WAC RRGB stereo panorama timeline sequence PC_WAC_STC_PAN captures images by using the Red (R) filter at the left Filter Wheel (FW); and Red, Green, Blue (RGB) filters of the right FW. For example, there are six PTU mast positions during Sol 6, whereas in Sol 7 it has twelve PTU positions, but in Sol 1 and Sol 8 both operate with ten positions. When the rover moves away from the landing site at Sol 22, the same timeline sequence will perform a 360° panorama. However, we only have one PTU

Digital Object Identifier 10.1109/MCI.2013.2279561
Date of publication: 16 October 2013

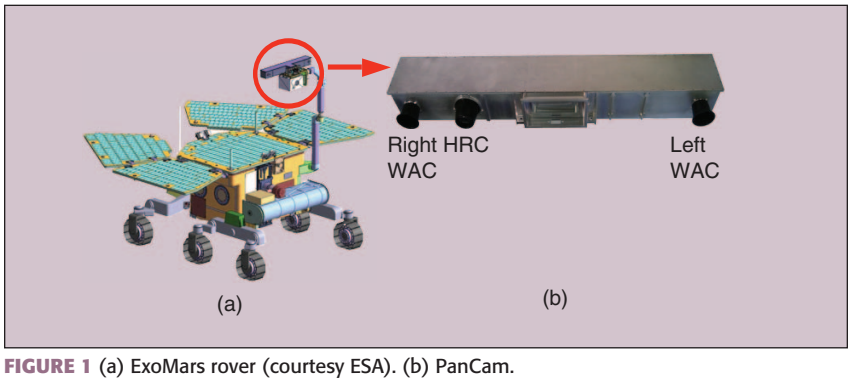

FIGURE 1 (a) ExoMars rover (courtesy ESA). (b) PanCam.

1556-603X/13/$31.00©2013IEEE

position in Sol 2 that allows our WAC to capture images with geology timeline sequence (PC_WAC_GL_PAN). Twelve geology filters apply in the order of L123456–R123456 where L represents left FW, R is right FW and 123456 are the corresponding filters. This timeline sequence also produces two WAC RR images simply by selecting the Red filter at each camera. Furthermore, we use one of these images to locate the next target for high resolution image acquisition. Figure 2(c) shows an HRC image as captured by the timeline sequence (PC_HRC_ALL_SEQ) during Sol 3, 4 and 10. On the other hand, HRC acquires 8 color images by using eight different PTU positions in Sol 1 and 2. Moreover, it is necessary to overlap the RGB filter subpositions at each PTU position, as shown in Figure 3, in order to construct an HRC color image.

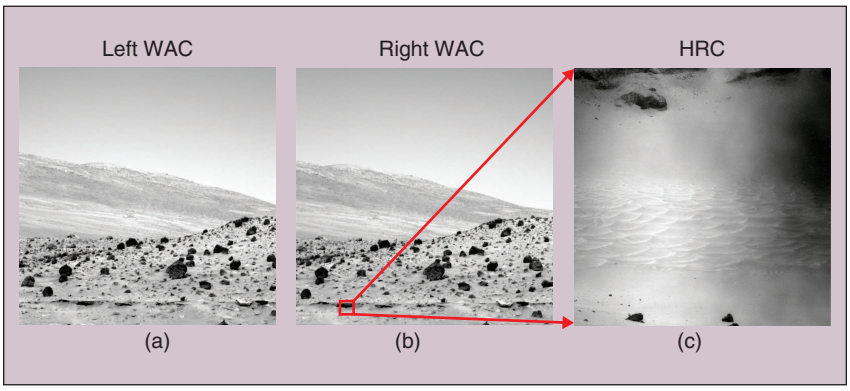

FIGURE 2 Shows Mars images (courtesy NASA) using PanCam simulator. (a) Left WAC. (b) Right WAC. (c) HRC.

II. PanCam

PanCam [16][25] is a space instrument operating in an environment that is hostile to humans and presently otherwise inaccessible, such as the surface of Mars. It has the operating temperature range from −45 °C to +30 °C; and it can also withstand the radiation of 4.2 krad. PanCam has two WAC and one HRC mounted on the optical bench (OB) that is located at the top of PTU, as shown schematically in Figure 4, which is 1.8 m above the ground. Left and right WAC are 500 mm (2 h in Figure 5) apart and operate as a stereo pair. It has 37° horizontal Field of View (FOV), focal length (f) of 22.5 mm, and individual FW for each camera; where FW contains 11 filters with wavelength (λ) between 440 nm and 1000 nm. Star-1000 one megapixel Active Pixel Sensors (APS) are selected for both WAC and HRC. HRC has a folded optical path to illuminate the APS, 5° horizontal FOV and focus at 150 mm. It uses blue, green and red stripe interference filter for color acquisition as shown in Figure 3. The blue and red filters occupy 341 pixels wide columns on the left and right edges of the APS. Our instrument has a single SpaceWire interface via the PanCam Interface Unit (PIU) which controls the cameras and FW. Primarily, PIU performs camera control, data handling, data communication to the rover and subsequently to Earth at the Rover Operations Control Centre (ROCC). PanCam software is written in C and LabVIEW as shown in Figure 6. It includes PanCam control panel in ROCC and PanCam functions as follows:

a) PanCam control panel
b) Timer delay function

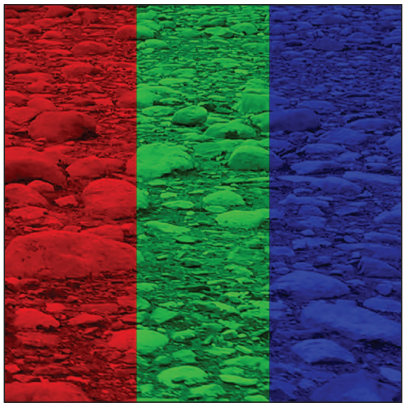

FIGURE 3 HRC RGB filter.

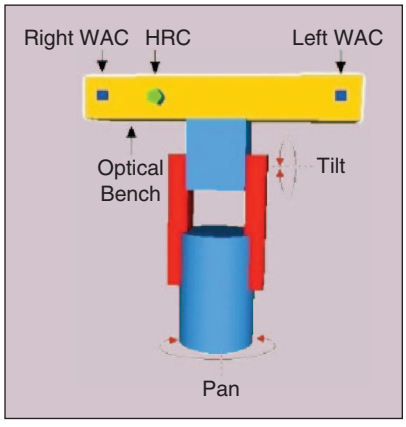

FIGURE 4 PanCam PTU.

TABLE 1 ExoMars rover PanCam timeline sequences.

TIMELINE SEQUENCE	Sol	TYPE	IMAGE	PTU
PC_WAC_STC_PAN	1, 8	WIDE-ANGLE STEREO RRGB	40	10
PC_WAC_STC_PAN	6	WIDE-ANGLE STEREO RRGB	24	6
PC_WAC_STC_PAN	7, 22	WIDE-ANGLE STEREO RRGB & PANORAMA	48	12
PC_WAC_GL_PAN	2	WIDE-ANGLE L123456-R123456 GEOLOGY FILTERS	12	1
PC_HRC_ALL_SEQ	1, 2	HIGH-RESOLUTION COLOR	8	8
PC_HRC_ALL_SEQ	3, 4, 10	HIGH-RESOLUTION COLOR	1	1

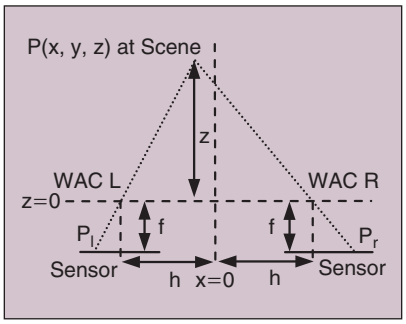

FIGURE 5 WAC stereo pair.

c) Timeline sequence
d) Exposure Time (ET)
e) Time stamp function
f) Filter control function
g) Autofocus, image capture and histogram.

III. PanCam Investigations

Our PanCam investigations were conducted in the Himalayas and at EBC according to ExoMars RSM. Note that the actual PanCam images are in 16 bit greyscale. The color images were taken by commercially available cameras to illustrate the characteristic of selected filters during the investigations. The results of investigations are listed as follows:

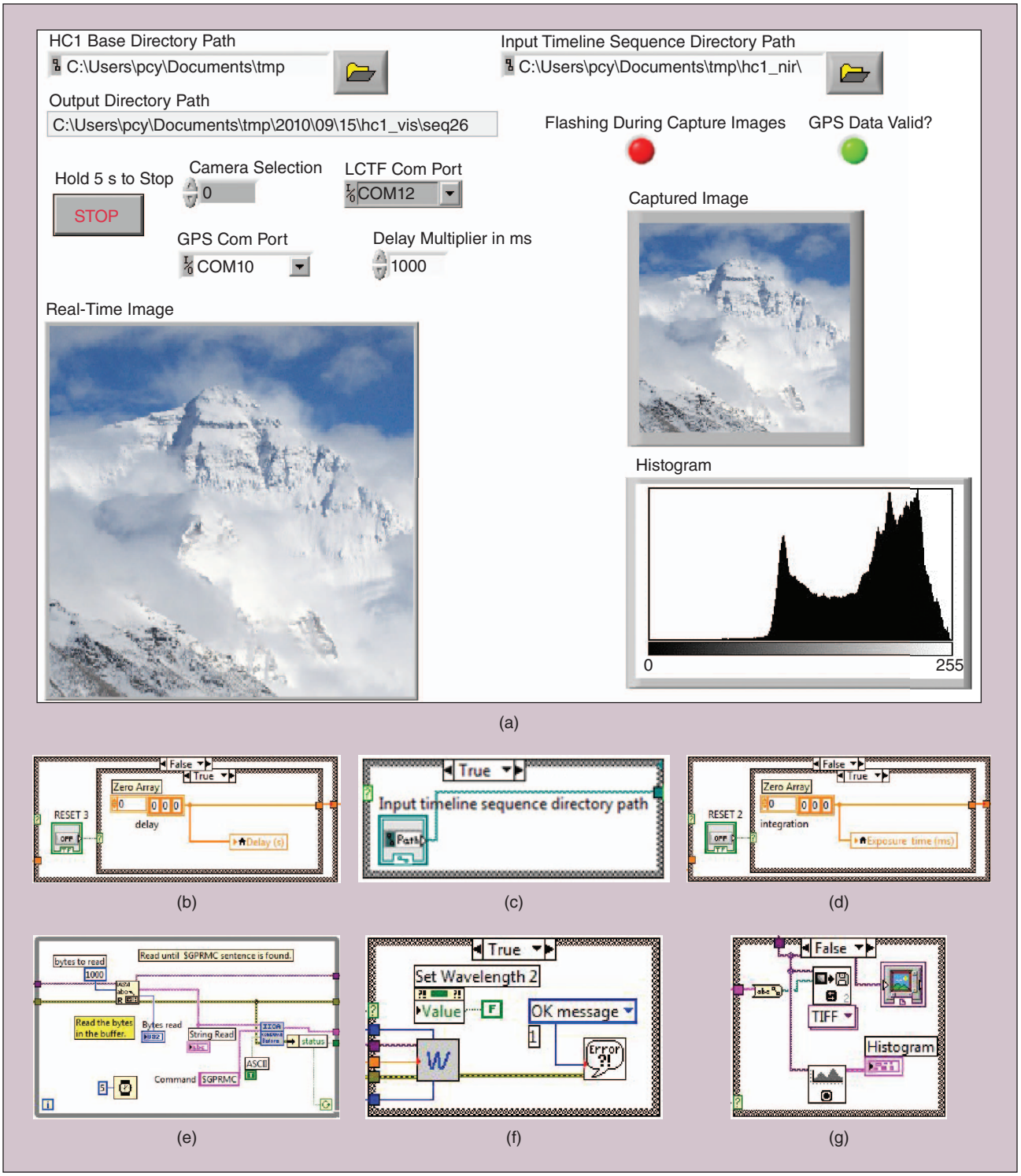

FIGURE 6 Shows (a) PanCam control panel at ROCC. (b)–(g) PanCam functions in LabVIEW.

TABLE 2 Investigation (1): using PC_WAC_STC_PAN.

WAC IMAGE ID		ET	λ
LEFT	RIGHT	(sec)	(nm)
(a) 45560		1.6	660
	(b) 45570	1.6	660
	(c) 45571	1.4	540
	(d) 45572	1.4	460

Investigation (1): Sol 1 highlighted results of WAC stereo color images using RRGB filters.

Investigation (2): Sol 1 eight HRC color images.

Investigation (3): Sol 2 WAC geology images using different filters.

Investigation (4): Sol 2 subset of HRC color images mosaic.

Investigation (5): Sol 6 six WAC stereo color images using RRGB filters.

Investigation (6): Sol 22 WAC color panorama images.

Investigation (1): Sol 1 Highlighted Results of WAC Stereo Color Images Using RRGB Filters

Images of EBC were acquired by the WAC at altitude 5,150 m with pan angle 20°, tilt angle 25°, toe in angle 2.8°, WVF 11.383 g/kg, ambient temperature 13 °C and pressure 483 hPa. The image resolution is 1024 × 1024. The first image acquired at 15:00 and took a total of 14 minutes to complete. Table 2 collects the subset of data. Figure 7 highlights the WAC stereo images with RRGB filters; (a) displays the image from left WAC with Red filter; (b), (c) and (d) are the images of right WAC with RGB filters; (e) is produced by combining (c) and (d); (f) shows the left and right color images from the scene for comparison. The final 3D stereo color anaglyph result image at (g) is generated from (a) and (e) images.

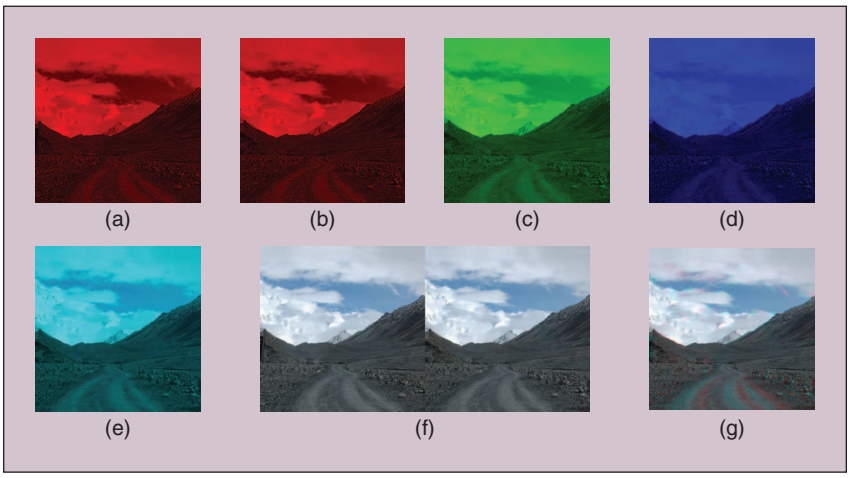

FIGURE 7 Shows investigation (1): WAC stereo images of rover tracks.

TABLE 3 Investigation (2): using PC_HRC_ALL_SEQ.

HRC IMAGE ID	PAN [deg]	TILT [deg]
(a) 49140	5	25
(b) 49141	10	25
(c) 49142	15	25
(d) 49143	20	25
(e) 49144	5	20
(f) 49145	10	20
(g) 49146	15	20
(h) 49147	20	20

TABLE 4 Investigation (3): using PC_WAC_GL_PAN.

WAC IMAGE ID		λ
LEFT	RIGHT	[nm]
(a) 47500		660
	(b) 47630	510
(c) 47510		540
	(d) 47650	470
(e) 47540		600
	(f) 47670	440
(g) 47560		560
	(h) 47690	720

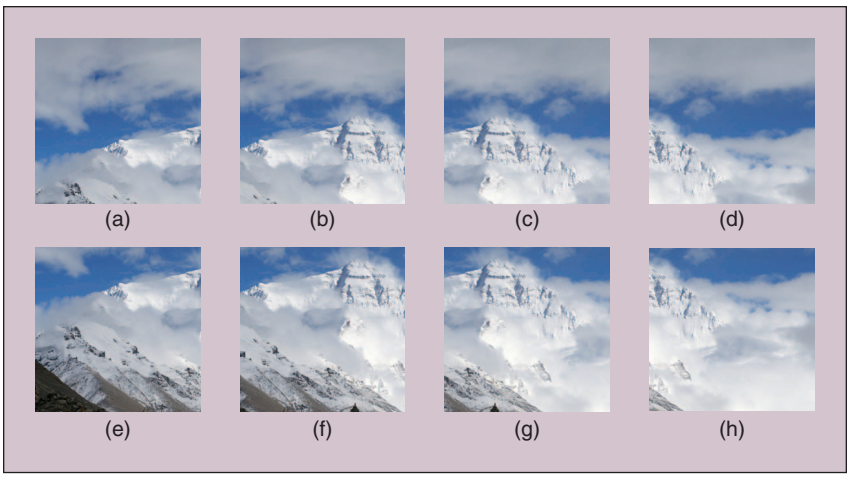

FIGURE 8 Shows investigation (2): Sol 1 eight HRC color images.

Investigation (2): Sol 1 Eight HRC Color Images

HRC captured the images of Mount Everest at 15:44, altitude 5,545 m, autofocus, ET 1.4 second, WVF 11 g/kg, ambient temperature 13 °C, pressure 483 hPa; and eight PTU positions as recorded in Table 3. Figure 8 illustrates the 1024 × 1024 resolution images; where images (b), (c), (f) and (g) are selected to experiment sub-framing, image compression, and super-resolution in Section IV.

Investigation (3): Sol 2 WAC Geology Images Using Different Filters

This investigation shows the geology images of Himalayan rocks at a single PTU position. Left and right WAC selected different geology filters to

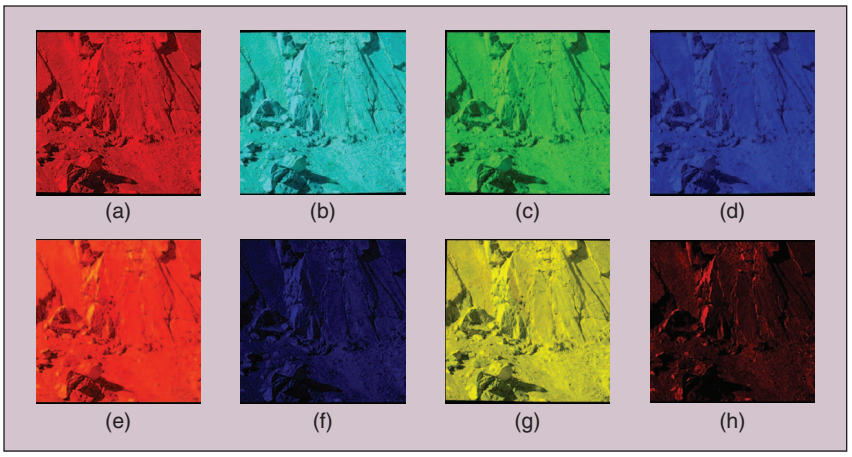

FIGURE 9 Shows investigation (3): Sol 2 WAC geology images.

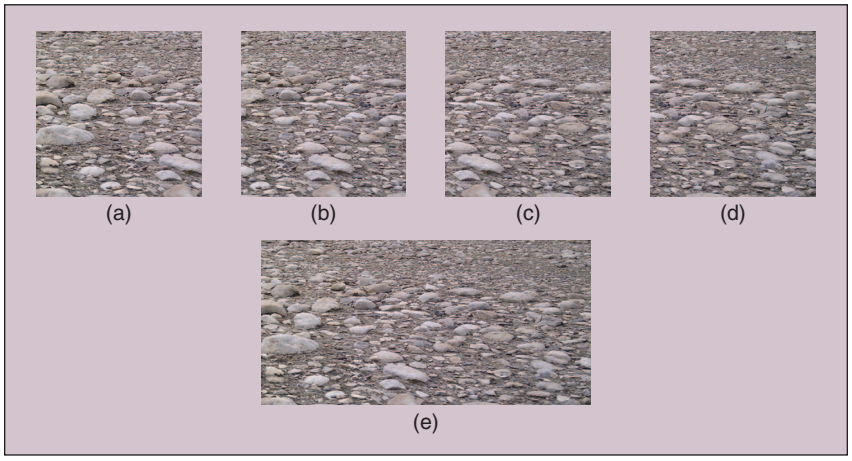

FIGURE 10 Shows investigation (4): Sol 2 HRC color images mosaic.

produce images at 1024 × 1024 resolution. These images were acquired during sunset at altitude 3,490 m, pan angle 10°, tilt angle 30°, toe in angle 2.8°, ET 1.6 second, WVF 16.673 g/kg, ambient temperature 37 °C and pressure 601 hPa. It took 5 minutes to complete. Table 4 includes the investigation data and Figure 9 displays the result images from the experiment. Note that the color images were acquired with a Beagle 2 left FW in front of an RGB camera; which had no IR-cut filter before the sensor.

Investigation (4): Sol 2 Subset of HRC Color Images Mosaic

Four 1024 × 1024 HRC images were acquired at EBC with altitude 5,150 m, tilt angle −20°, autofocus, ET 1.4 second WVF 11.383 g/kg, ambient temperature 13 °C and pressure 483 hPa. The investigation started at 15:28. Table 5 and Figure 10 (a), (b), (c) and (d) show the recorded data and images. Figure 10 (e) illustrates the result of HRC color images mosaic as displayed at the ROCC.

Investigation (5): Sol 6 Six WAC Stereo Color Images Using RRGB Filters

WAC accomplished the PC_WAC_STC_PAN timeline sequence successfully; and captured twenty-four images in the Himalayan region at altitude 3,490 m. During each PTU position, we acquired 1024 × 1024 resolution RRGB images at the tilt angle 15°, toe in angle 2.8°; which had the similar imaging results as described in Figure 7. Table 6 collects the data during the timeline sequence. Note that abbreviation AT represents ambient temperature and Pres is pressure in the following tables.

TABLE 5 Investigation (4): using PC_HRC_ALL_SEQ.

HRC IMAGE ID	PAN [deg]
(a) 02670	12.5
(b) 02671	15.0
(c) 02672	17.5
(d) 02673	20.0

Investigation (6): Sol 22 WAC Color Panorama Images

Twelve WAC RGB images were captured in the Himalayas at altitude 3,490 m with resolution 1024 × 1024, tilt angle 30° and toe in angle 2.8°. This panorama timeline sequence was completed successfully. Table 7 and Figure 11 display the result data and panoramic view of WAC RGB images.

IV. Sub-Framing, Data Compression and Super-Resolution

ExoMars PanCam image compression is a robust wavelet algorithm [5]. It has the lossless and lossy compressions which provide either high definition images for close examination or heavily compressed thumbnail images for efficient transmission. Primarily, the data volume of WAC or HRC image is determined by the compression ratio, sub-framing (cropping) size and image resolution (e.g. down-sampling) from the lossless compression ratio 2:1 (8 bit per pixel) to the lossy compression 80:1 (0.2 bit per pixel) thumbnail. There are six different sizes of image including 1024, 512, 256, 128, 64 and 32 pixels in row and column, Assuming the row value is equal to the column, rover normally keeps 10:1 (1.6 bit per pixel) compressed image in memory for the general geological investigation and scientific purposes. The highly compressed thumbnail (i.e. quick look, preview) often leads to the next download for the same image but with a higher resolution. In general, image data should be compressed before packetizing and transmitting to the ROCC; very occasionally it may be desirable to transmit an uncompressed raw image. In this case, additional image processing functions such as down-sampling,

sub-framing and super-resolution should be considered for saving data volume.

The need to transmit a lossless (2:1) compressed image is extremely rare. However, if it is required, the image sub-framing and super-resolution techniques for each individual object (e.g. rocks, landmarks) from the scene should be considered as an option to reduce the image size and data volume. Figure 12 shows the results of sub-framing and super-resolution at the lossless compression ratios. Figure 13 provides the use case diagram of the sub-framed at the Region of Interest (ROI), compression and super-resolution. The algorithm is defined as follows:

1) Telecommand to PanCam to capture image at the scene from Mars.
2) Generate thumbnail (80:1 compression ratio) from image.
3) Downlink the thumbnail to the ROCC.
4) ROCC decompresses the thumbnail.
5) Select the ROI (e.g. 256 × 256) from the thumbnail.
6) Uplink the ROI coordinates to rover via a timeline sequence.
7) Use the defined coordinates to command PTU and PanCam to take 4 images from the scene iteratively.
8) Sub-framing the ROI at the images.
9) Perform the lossless data compression (2:1) on the sub-framed images.
10) Downlink the compressed sub-framed images to the ROCC.
11) ROCC decompresses the images.
12) ROCC applies the super-resolution algorithm to the images to re-construct a high resolution image.

TABLE 6 Investigation (5): using PC_WAC_STC_PAN.

WAC IMAGE ID		TIME	PAN	ET	λ	WVF	AT	PRES
LEFT	RIGHT	(hr:min)	(deg)	(sec)	(nm)	(g/kg)	(°C)	(hPa)
45860		12:14	20	1.6	660	12.711	23	603
	45890			1.6	660			
	45891			1.4	540			
	45892			1.4	460			
45940		12:28	40	1.6	660	13.370	25	602
	45960			1.6	660			
	45961			1.4	540			
	45962			1.4	460			
46010		12:42	60	1.6	660	13.956	27	601
	46030			1.6	660			
	46031			1.4	540			
	46032			1.4	460			
46090		12:56	80	1.6	660	14.011	29	600
	46110			1.6	660			
	46111			1.4	540			
	46112			1.4	460			
46160		13:10	100	1.6	660	13.940	30	600
	46181			1.6	660			
	46182			1.4	540			
	46183			1.4	460			
46230		13:24	120	1.6	660	14.780	31	600
	46250			1.6	660			
	46250			1.4	540			
	46250			1.4	460			

V. Design Methodology of Autonomous and Computational Intelligent System for the Rover

PanCam operates from Earth by radio link, where because of the delays in communication due to the great distance involved, real-time operation is impossible. Figure 13 shows the selection of ROI demanding actions from the ROCC. To perform such operation we need human intervention and decision making which could take at least one Sol to complete the task. Although an optional automatic PanCam image capture software is available for targeting rigid objects like rocks, the rover is not equipped to detect free-form objects; such as dust devils and other astronomical events on Mars. Hence, an alternative approach becomes necessary, especially when it is operating under extreme hostile environment. We introduce a novel design methodology of autonomous and computational intelligent system for the rover, which is called Mission-Specific Data Processor (MSDP), a system based on the flexible architectural approach for multi-disciplinary applications in the aerospace industry. MSDP simplifies the overall operations in the rover. It caters for multi-channel input and processes data in real-time on-board the rover according to user-defined scenarios. For example, the rover's housekeeping channel records the mission-specific information for analysis and reports failures as a part of self-learning computational intelligent system (i.e. autonomous mission-specific rover output). MSDP divides the output data into different levels. It enables multi-tasking process for data fusion and multi-node system architecture for the image database. Other database handles a set of multi-disciplinary telecommands and telemetry based on a scenario to provide data information such as rover coordinates, navigation parameters and path planning. Another database that supplies the data processing algorithms including image processing, segmentation and representation [28], feature extraction and matching [29], object detection and recognition [19], self-learning and training. At each level of output, a data logger tracks the data passing through

TABLE 7 Investigation (6): using PC_WAC_STC_PAN.

WAC IMAGE ID		TIME	PAN	ET	λ	WVF	AT	PRES
LEFT	RIGHT	(hr:min)	(deg)	(sec)	(nm)	(g/kg)	(°C)	(hPa)
46370		14:00	0	1.6	660	15.378	35	606
	46390			1.6	660			
	46391			1.4	540			
	46392			1.4	460			
46480		14:14	5	1.6	660	18.575	37	606
	46500			1.6	660			
	46501			1.4	540			
	46502			1.4	460			
46590		14:28	10	1.6	660	19.711	38	604
	46620			1.6	660			
	46621			1.4	540			
	46622			1.4	460			
46670		14:42	15	1.6	660	19.591	40	604
	46690			1.6	660			
	46691			1.4	540			
	46692			1.4	460			
46740		14:56	20	1.6	660	20.051	42	604
	46770			1.6	660			
	46771			1.4	540			
	46772			1.4	460			
46820		15:10	25	1.6	660	20.330	44	604
	46840			1.6	660			
	46841			1.4	540			
	46842			1.4	460			
46890		15:24	30	1.6	660	20.389	45	604
	46920			1.6	660			
	46921			1.4	540			
	46922			1.4	460			
47040		15:38	35	1.6	660	20.388	46	604
	47060			1.6	660			
	47061			1.4	540			
	47062			1.4	460			
47150		15:52	40	1.6	660	19.371	45	603
	47180			1.6	660			
	47181			1.4	540			
	47182			1.4	460			
47230		16:06	45	1.6	660	20.423	46	603
	47250			1.6	660			
	47251			1.4	540			
	47252			1.4	460			
47300		16:20	50	1.6	660	20.423	46	603
	47320			1.6	660			
	47321			1.4	540			
	47322			1.4	460			
47370		16:34	55	1.6	660	19.315	46	603
	47390			1.6	660			
	47391			1.4	540			
	47392			1.4	460			

the current level. A synchronisation process safeguards the integrity of the data sets. Figure 14 shows the autonomous MSDP architectural design.

A. Visual Data Fusion (VDF)

VDF is a software engine which ingests multiple visual inputs to produce more accurate and complete 3D data products, such as nested multi-resolution digital terrain maps [20], texture maps, and a constantly updated location map [14]. In a Geographic Information System (GIS) context, data fusion is often simply considered as a data interpolation from different sensors to enhance the spatial resolution (or the coverage) of the reconstructed site of interest. However, in many cases, it includes a process to produce a more accurate data product by fusing multiple estimation results with different levels of statistical confidence. Assuming a global positioning system-free (and possibly inertial measurement unit-free) environment where visual information is the vital clue to compensate for the error involved in the mechanical odometers for localization, data fusion is an important process for any autonomous rover which contains more than one range sensor. Nevertheless, most rover applications to date have overlooked the significance of such data fusion because each sensor has been developed for a specific purpose. Although in robotics it is commonplace to fuse information from the same sensors by a Simultaneous Localization and Mapping (SLAM) technique [1], this is restricted to the results from the same sensor in most cases. Data fusion with overview(s) from different platforms has not been properly investigated to date by anyone. Furthermore, if there is a dedicated Geographical Image Database Server (GIDS) that stores the sensed data and its derived data products, it is possible to design a more aggressive data fusion process, which can refine a current reconstruction/location by the previous sensing results at different positions. Thus, one of the core technologies, developed by the data fusion process is a robust image matcher via a new matching feature from 2D–3D data fusion. In addition, considering a situation to fuse reconstruction

results from rear and front views, 3D model-based data matching plays an important role in the fusion. Fast 3D model-based searching within a large GIDS database is another significant challenge, in which we have considerable experience and knowledge.

B. Learning-Enabled Object Detection (LOD)

LOD provides the ability to perceive surrounding objects by extracting meaningful information from sensor data, and is the key to autonomous systems. This is especially true for localizing and navigating unmanned vehicles; such as a rover in a dynamic environment. Rock-like objects can be classified as hazards that could potentially obstruct the rover's path; landmarks that can be used as reference points for localization and building maps, or ROI, or scientifically important rocks on Mars. Objects can be retrieved by processing various types of sensor data but we focus here on images from PanCam. Current vision-based methods of detecting and classifying objects are based on the object's geometric features and appearance. The dominant approaches for real-time processing of objects use holistic generative and discriminative models [24]. Generative holistic models are suitable for recognizing objects with relatively uniform geometric properties (e.g. pipes, faces) whereas discriminative models work best with previous knowledge of the appearance of the object that is stored in a template during training. Naturally, discriminative models run faster but are restricted by the available templates. Our object detection is achieved by processing and fusing data from multiple sensors including images captured by PanCam.

C. Self-Learning Agent (SLA)

SLA is capable of inferring objects from partial knowledge of the detected features by utilizing a multitude of data processing techniques. The SLA employs a hierarchical approach where class descriptions are learnt based on the complexity of the classification method as described in Figure 15. A template of object classes is stored and updated in the Environment Model Library (EML) upon successful detection

FIGURE 11 Shows investigation (6): Sol 22 WAC panorama.

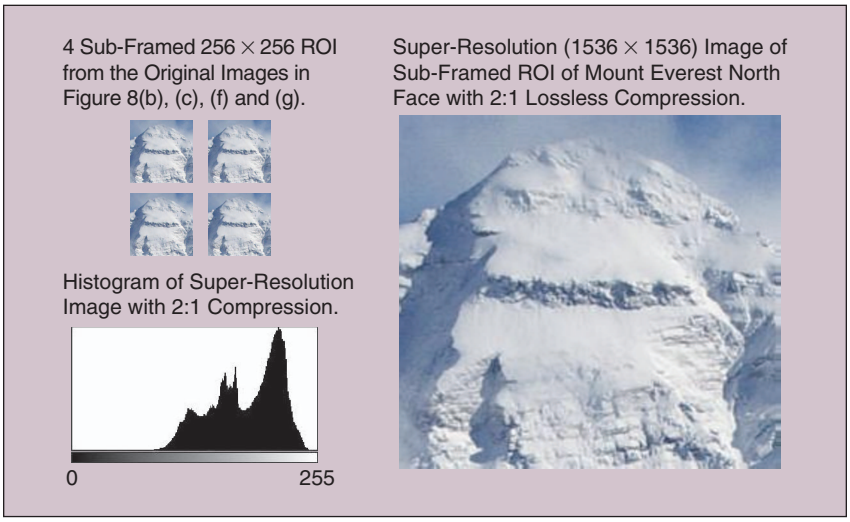

FIGURE 12 Shows sub-framed ROI, compression and super-resolution.

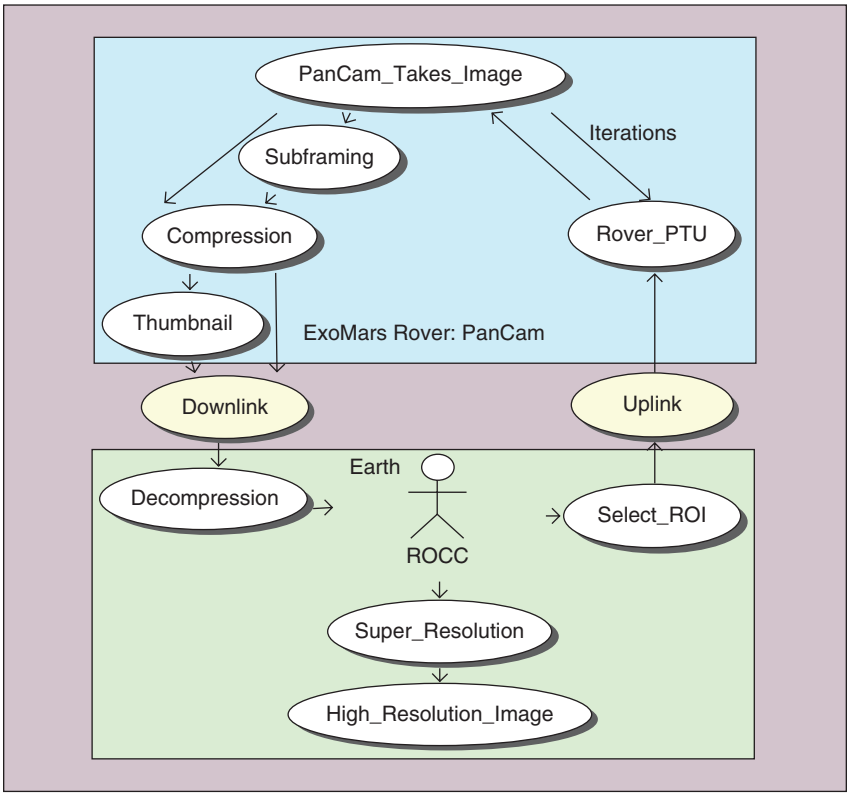

FIGURE 13 The use case diagram.

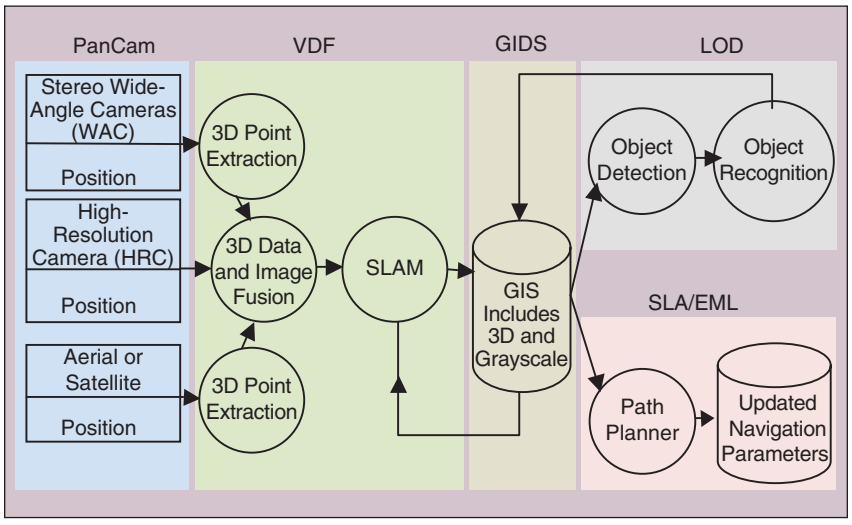

FIGURE 14 Shows the autonomous and computational intelligent MSDP architecture.

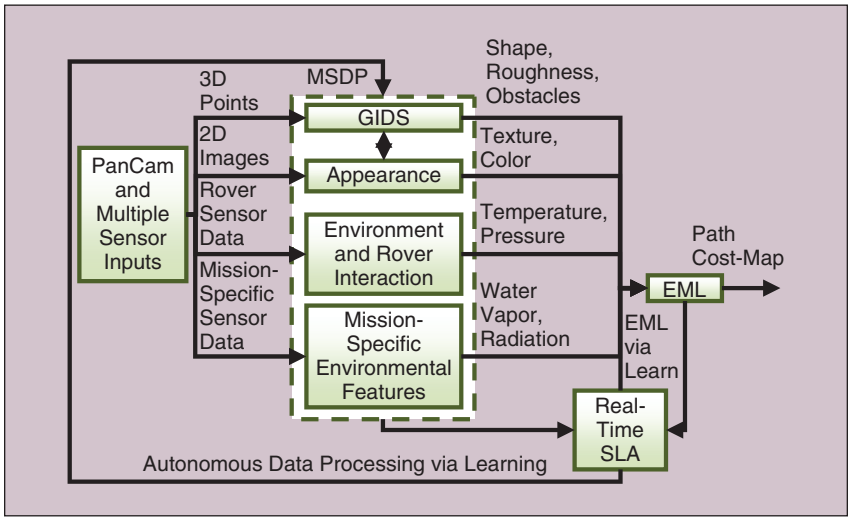

FIGURE 15 Shows the rover autonomous data processing via learning.

of the object in question, so as to increase the identification speed of similar objects and to reduce the load on computational resources. The main challenges here are to achieve learning in real time and to improve object detection speed and robustness. The existing data mining and learning techniques applied in other applications such as search engines are relevant but not readily or directly applicable.

Hence, for the benefits of the design of SLAM and LOD, a self-organizing map with neural networks adequately classifies the sensor outputs during the learning process [12]. Using geometric hashing for the abstract features in 3D space [18], the neurons in the lattice generate the self-organizing feature map. According to the topological order, the learning algorithm of the self-organized map is outlined as follows:

1) Randomly select a weighted value from the neurons.
2) Pick three sample points from the 3D space.
3) Matching through all neurons according to the given weighted value to find the winning neurons.
4) Update the weighted value from the winning neurons.
5) Iterate the process from step (2) until it becomes a steady state.

Most importantly the learning rate of SLA depends on the size of kernel that we convolve to find the features of curvature class and torsion class within the neighborhood of local surface. Similarly, this applies to the other classes such as roughness, obstacles, texture, color, temperature, pressure, water vapor and radiation as defined in Table 6 and Table 7.

D. Environment Model Library (EML)

EML consists of detected objects and environment properties that are mapped with the location information from the GIDS. The library is the result of multiple pipeline processes [8][23] shown in Figure 15 and provides a solution for autonomous navigation [4][11] and environment perception. Objects can be abstracted in various classes based on; for example, geometry, appearance and material attributes. As the autonomous rover interacts with the environment, the library offers a database of human-like interpretation of the environment. This in turn allows the rover to make human-like decisions [26], such as producing a path cost-map that is optimized based on the EML and can be used for path planning of the rover as given in Figure 16. SLA is responsible for comparing the partial information obtained during the detection stage with data within the EML to achieve classification. If required, data from the EML can also be displayed from a 3D virtual reality simulator at the ROCC such as the one presented in [27]. This concept can increase learning accuracy by incorporating human feedback in a timely manner.

VI. Conclusions and Future Research

Our investigations in the Himalayas and at Mount Everest provided useful information for PanCam and for future R&D. Capturing images according to the ExoMars rover baseline information in the RSM gave us the opportunities to explore how the planning works when the rover interacts under hostile environment. Mount Everest provides a good analogue for an excursion on the surface of Mars [10]. For example, using the captured WAC stereo images we have successfully re-constructed the 3D stereo images of Mars-like-landscapes at EBC. Furthermore, we demonstrated that the data volume can be significantly reduced with minimum loss in its image quality after sub-framing, data compression and super-resolution. Finally, the novel MSDP

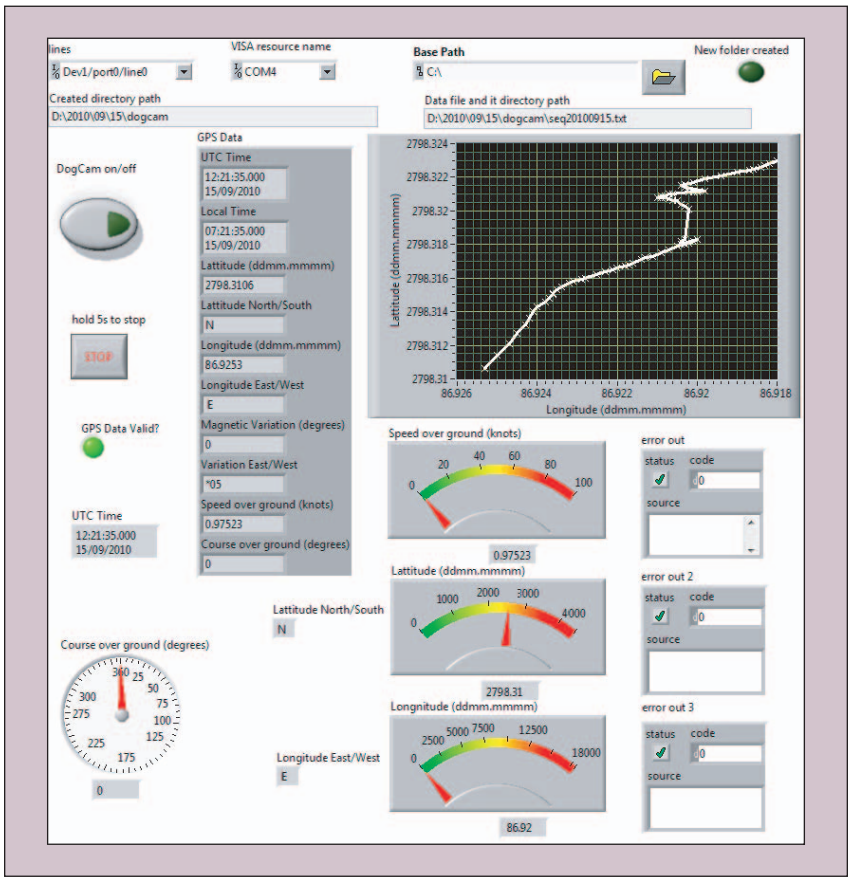

FIGURE 16 Shows the camera guided, navigation path for rover.

approach allows us to improve the current ExoMars rover PanCam functionality; and to expand its future applications for autonomy and computational intelligence [3][17] in space science [30].

Acknowledgment

ExoMars PanCam is funded by UKSA. The authors especially thank UKSA's support throughout the PanCam R&D. The authors would like to thank the ExoMars PanCam team members from ESA, Thales Alenia Space, Astrium, Deutsches Zentrum für Luft und Raumfahrt e.V., SPACE-X, Kayser-Threde, Aberystwyth University, Joanneum Research, Surrey Space Centre and MSSL for their contributions to this project.

References

[1] R. Abielmona, E. M. Petriu, M. Harb, and S. Wesolkowski, "Mission-driven robotic intelligent sensor agents for territorial security," *IEEE Comput. Intell. Mag.*, vol. 6, no. 1, pp. 55–67, 2011.

[2] D. A. Alexander, R. G. Deen, P. M. Andres, P. Zamani, H. B. Mortensen, A. C. Chen, M. K. Cayanan, J. R. Hall, V. S. Klochko, O. Pariser, C. L. Stanley, C. K. Thompson, and G. M. Yagi, "Processing of mars exploration rover imagery for science and operations planning," *J. Geophys. Res.*, vol. 111, no. E02S02, 2006.

[3] I. Arel, D. C. Rose, and T. P. Karnowski, "Deep machine learning—A new frontier in artificial intelligence research," *IEEE Comput. Intell. Mag.*, vol. 5, no. 4, pp. 13–18, 2010.

[4] J. J. Biesiadecki and M. W. Maimone, "The mars exploration rover surface mobility flight software: Driving ambition," *IEEE Aerospace Conf. Proc. 5*, Big Sky, MT, Mar. 2006.

[5] M. Cabral, "WhiteDwarf compression tester user's manual," TEC-EDP, European Space Agency, Noordwijk, The Netherlands, Tech. Rep., 2009.

[6] D. Coulter and T. Phillips, "NASA heads up Mt. Everest," Science NASA, Washington, D.C., Tech. Rep., 2009.

[7] Y. Gao, "Optical flow based techniques for ExoMars rover autonomous navigation," in *Proc. Int. Symp. Artificial Intelligence, Robotics Automation Space*, Los Angeles, CA, Feb. 2008.

[8] Y. Gao, R. Samperio, K. Shala, and Y. Cheng, "Modular design for planetary rover autonomous navigation software using ROS," *Acta Futura*, no. 5, pp. 9–16, 2012.

[9] A. D. Griffiths, A. J. Coates, R. Jaumann, H. Michaelis, G. Paar, D. Barnes, J-L. Josset, J. Oberst, J. Albertz, J. P. Bibring, I. Crawford, A. Ellery, B. Foing, V. Formisano, S. V. Gasselt, R. Gowen, E. Hauber, H. Hoffmann, B. A. Hofmann, Y. Langevin, R. Li, W. Markiewicz, P. Masson, S. Mottola, J-P. Muller, D. Pullan, P. Reuffer, T. Spohn, N. Thomas, and R. Trautner, "Context for the ESA ExoMars rover: The panoramic camera (PanCam) instrument," *Int. J. Astrobiol.*, vol. 5, no. 3, pp. 269–275, 2006.

[10] P. Hodge, *Higher than Everest: An Adventurer's Guide to the Solar System*. Cambridge, U.K.: Cambridge Univ. Press, 2001.

[11] F. Ingrand, S. Lacroix, S. Lemai-Chenevier, and F. Py, "Decisional autonomy of planetary rovers," *J. Field Robot.*, vol. 24, no. 7, pp. 559–580, 2007.

[12] B. Jähne and H. Haußecker, *Computer Vision and Applications*. New York: Academic Press, 2000, ch. 17, pp. 577–606.

[13] R. Li, S. W. Squyres, R. E. Arvidson, B. A. Archinal, J. Bell, Y. Cheng, L. Crumpler, D. J. Des Marais, K. Di, T. A. Ely, M. Golombek, E. Graat, J. Grant, J. Guinn, A. Johnson, R. Greeley, R. L. Kirk, M. Maimone, L. H. Matthies, M. Malin, T. Parker, M. Sims, L. A. Soderblom, S. Thompson, J. Wang, P. Whelley, and F. Xu, "Initial results of rover localization and topographic mapping for the 2003 mars exploration," *Photogramm. Eng. Remote Sens.*, vol. 71, no. 10, pp. 1129–1142, 2005.

[14] R. Li, K. Di, A. B. Howard, L. Matthies, J. Wang, and S. Agarwal, "Rock modeling and matching for autonomous long-range mars rover localization," *J. Field Robot.*, vol. 24, no. 3, pp. 187–203, 2007.

[15] R. Li, W. Wang, D. Li, O. Karahayit, P. Tang, A. J. Coates, J.-P. Muller, A. D. Griffiths, G. Paar, and J. Oberst, "ESA ExoMars rover pancam prelaunch modeling and accuracy assessment for localization and topographic mapping," in *Proc. European Planetary Science Congr.*, 2012, vol. 5, p. 252.

[16] J. N. Maki, J. F. Bell III, K. E. Herkenhoff, S. W. Squyres, A. Kiely, M. Klimesh, M. Schwochert, T. Litwin, R. Willson, A. Johnson, M. Maimone, E. Baumgartner, A. Collins, M. Wadsworth, S. T. Elliot, A. Dingizian, D. Brown, E. C. Hagerott, L. Scherr, R. Deen, D. Alexander, and J. Lorre, "Mars exploration rover engineering cameras," *J. Geophys. Res.*, vol. 108, no. E12, pp. ROV 12–1, 2003.

[17] H. P. Martínez, Y. Bengio, and G. N. Yannakakis, "Learning deep physiological models of affect," *IEEE Comput. Intell. Mag.*, vol. 8, no. 2, pp. 20–33, 2013.

[18] F. Mokhtarian, N. Khalili, and P. Yuen, "Free-form 3-D object recognition at multiple scales," in *Proc. 11th British Machine Vision Conf.*, 2000, pp. 446–455.

[19] F. Mokhtarian, N. Khalili, and P. Yuen, "Multi-scale free-form 3D object recognition using 3D models," *Image Vis. Comput.*, vol. 19, no. 5, pp. 271–281, 2001.

[20] C. F. Olson, L. H. Matthies, J. R. Wright, R. Li, and K. Di, "Visual terrain mapping for Mars exploration," *Comput. Vis. Image Understanding*, vol. 105, no. 1, pp. 73–85, 2007.

[21] M. R. Patel, J. C. Zarnecki, and D. C. Catling, "Ultraviolet radiation on the surface of Mars and the Beagle 2 UV sensor," *Planet. Space Sci.*, vol. 50, no. 9, pp. 915–927, 2002.

[22] C. Qiang, C. Tao, and Q. Zheng, "Research on motion planning based on self-learning behavior agent for AUV," in *Proc. IEEE Int. Conf. Mechatronics Automation*, 2009, pp. 4440–4445.

[23] K. Shala and Y. Gao, "Review and analysis of localization and mapping techniques for planetary rovers," in *Proc. 10th Int. Symp. Artificial Intelligence, Robotics Automation Space*, Japan, Aug.–Sept. 2010.

[24] D. L. Sancho-Pradel and Y. Gao, "A survey on terrain assessment techniques for autonomous operation of planetary robots," *J. Br. Interplanet. Soc.*, vol. 63, nos. 5–6, pp. 206–217, 2010.

[25] M. Woods, A. Shaw, D. Barnes, D. Price, D. Long, and D. Pullan, "Autonomous science for an ExoMars Rover-like mission," *J. Field Robot*, vol. 26, no. 4, pp. 358–390, 2009.

[26] R. Yan, K. P. Tee, Y. Chua, H. Li, and H. Tang, "Gesture recognition Based on localist attractor networks with application to robot control," *IEEE Comput. Intell. Mag.*, vol. 7, no. 1, pp. 64–74, 2012.

[27] C. Yu, H. Ju, and Y. Gao, "3D virtual reality simulator for planetary Rover operation and testing," in *Proc. IEEE Int. Conf. Virtual Environment, Human-Computer Interfaces, Measurement Systems*, 2009, pp. 101–106.

[28] P. Yuen, F. Mokhtarian, and N. Khalili, "Multi-scale 3-D surface description: Open and closed surfaces," in *Proc. Scandinavian Conf. Image Analysis*, 1999, pp. 303–310.

[29] P. Yuen, F. Mokhtarian, N. Khalili, and J. Illingworth, "Curvature and torsion feature extraction from free-form 3-D meshes at multiple scales," *IEE Proc. Vision, Image Signal Processing*, vol. 147, no. 5, pp. 454–462, 2000.

[30] P. Yuen, "Knowledge transfer in space science," in *Proc. 5th Int. Conf. Knowledge Management Asia Pacific 11th Int. Symp. Knowledge Systems Sciences*, Sept. 16–18, 2010.